ELSEVIER

Contents lists available at ScienceDirect

### Journal of Solid State Chemistry

journal homepage: www.elsevier.com/locate/jssc



# Post-growth thermal oxidation of wurtzite InN thin films into body-center cubic In<sub>2</sub>O<sub>3</sub> for chemical/gas sensing applications



H.F. Liu<sup>a,\*</sup>, N.L. Yakovlev<sup>a</sup>, D.Z. Chi<sup>a</sup>, W. Liu<sup>b</sup>

- <sup>a</sup> Institute of Materials Research and Engineering (IMRE), A\*STAR (Agency for Science, Technology and Research), 3 Research Link, Singapore 117602, Singapore
- <sup>b</sup> School of Electrical and Electronic Engineering, Luminous! Center of Excellence for Semiconductor Lighting and Display, Nanyang Technological University, Singapore 639798, Singapore

#### ARTICLE INFO

Available online 18 October 2013

Keywords: Body-center cubic In<sub>2</sub>O<sub>3</sub> InN thin films Rapid thermal annealing Epitaxial oxidation MOCVD

#### ABSTRACT

Post-growth thermal oxidations of InN have been studied using high-resolution x-ray diffraction (HRXRD) and secondary ion-mass spectroscopy (SIMS). The InN thin films, having relative high crystal quality, were grown by metal-organic chemical vapor deposition (MOCVD) on c-sapphire substrates using InGaN/GaN buffer layers. HRXRD reveals that oxidation of wurtzite InN into body-center cubic  $\ln_2O_3$  occurred at elevated temperatures. A  $Si_3N_4$  encapsulation improves the crystal quality of  $\ln_2O_3$  oxidized by using conventional rapid thermal annealing (RTA) but it results in the presence of undesired metallic indium. Cycle-RTA not only improves the crystal quality but also avoids the byproduct of metallic indium. SIMS depth profile, using contaminate elements as the 'interface markers,' provide evidence that the oxidation of InN is dominated by oxygen inward diffusion mechanism. Together with the HRXRD results, we conclude that the crystal quality of the resultant  $\ln_2O_3/InN$  heterostructure is mainly controlled by the balance between the speeds of oxygen diffusion and InN thermal dissociation, which can be effectively tuned by cycle-RTA. The obtained  $\ln_2O_3/InN$  heterostructures can be fundamental materials for studying high speed chemical/gas sensing devices.

© 2013 Elsevier Inc. All rights reserved.

#### 1. Introduction

III-oxides, typically In<sub>2</sub>O<sub>3</sub> and Ga<sub>2</sub>O<sub>3</sub>, are functional materials that have various applications in chemical and/or gas sensing devices [1–3]. Integration of III-oxide based sensors and III-nitride based high speed transistors has the potential to improve the sensing speed and thus widely broadens its applications. Although thermal oxidation of III-nitrides, replacing the deposition of "foreign" dielectrics, is of fundamental and practical interest for the fabrication of GaN-based electronic devices, e.g., metal–oxide–semiconductor heterojunction field effect transistors (MOS-HFETs) [4], there exists great challenges to obtain high quality oxide insulator via postgrowth oxidation of GaN or AlN [5]. However, alloying of In into GaN and AlN, forming InGaN and AlInN ternary compounds, respectively, can somehow facilitate the oxidation process. For example, nearly native Al<sub>2</sub>O<sub>3</sub> oxide layer can be obtained by thermal oxidation of Al<sub>0.87</sub>In<sub>0.13</sub>N [6,7].

On the other hand, InN was predicted to have higher mobility than GaN and AlN when the electrical field is lower than 100 kV/cm [8]. The saturated velocity of InN (at the electric field of 65 kV/cm) is

\*Corresponding author. Tel.: +65 68748047. E-mail address: liuhf@imre.a-star.edu.sg (H.F. Liu). also higher than those of GaN and AlN (at the electric field of 140 and 450 kV/cm, respectively) [8]. In the last few years, the crystal quality of InN thin films grown by metal–organic chemical vapor deposition (MOCVD) has greatly improved [9,10], which makes the fabrication of InN-based high speed electronic device practical and realizable. In this regard, thermal oxidation of an InN/AlInN/InN multilayer structure grown on a GaN template to convert the InN/AlInN on top into  $In_2O_3/Al_2O_3$  can monolithically integrate the  $In_2O_3$ -based chemical and/or gas sensing devices with the InN-based high speed transistors by automatically locating the  $In_2O_3$  sensor on the  $Al_2O_3$  gate material. In this way, the sensitivity as well as the sensing speed of the device can be largely increased without any requirements of re-growth [11]. To push forward this idea toward practice, we have studied postgrowth thermal oxidation of InN thin films that were epitaxially grown

on c-plane sapphire substrates by MOCVD using InGaN/GaN buffer layers. For these studies we have employed high-resolution x-ray diffraction (HRXRD) and secondary ion-mass spectroscopy (SIMS).

#### 2. Experiments

The InN thin films of 180 nm were grown at 600 °C by MOCVD on c-plane sapphire substrates using InGaN/GaN buffer layers, the

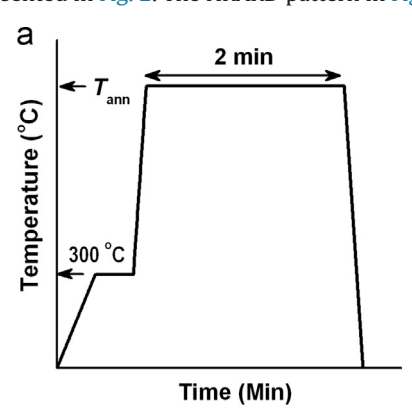
detailed growth procedures can be found in our earlier publications [9,10]. The InGaN buffer, 50 nm in thickness grown at 720 °C, is to bridge the large lattice mismatch between InN and GaN so as to improve the crystal quality of the following growth of InN. As a result, the full-width at half-maximum (FWHM) of the InN (0 0 0 2) HRXRD rocking curve is reduced from 1.25° to 0.89° by the InGaN buffer layer while keeping, otherwise, the same growth conditions. The electron density and the electron mobility of the InN thin films measured by Hall-effect at room temperature are around  $2.4 \times 10^{19}$  cm $^{-3}$  and 235 cm $^2$ /V s, respectively.

For the post-growth thermal oxidation, the InN thin film samples were diced into small pieces in square (8  $\times$  8 mm). Si $_3$ N $_4$  coating, when required, was done using a plasma-enhanced chemical vapor deposition (PECVD) system. The thermal oxidation was carried out at different temperatures in a rapid thermal annealing (RTA) chamber under flowing N $_2$  atmosphere. No intentional oxygen was supplied during the thermal oxidation. Two methods of annealing, i.e., conventional RTA and cycle-RTA (CRTA) which are schematically shown in Fig. 1(a) and (b), respectively, were employed for the thermal oxidation. The target annealing temperatures ( $T_{\rm ann}$ ) were set in the range from 650 to 750 °C.

Structural evolution of the InN thin film at various thermal oxidation conditions was characterized using Cu- $K\alpha_1$  HRXRD in the standard  $\omega$ - $2\theta$  geometry. SIMS was carried out by using a time-of-flight mass spectrometer (ION-TOF GmbH). Ar (1 kV) and Bi (25 kV) were used as the sputtering and analysis beams, respectively. Positive secondary ions were collected not only for the intrinsic elements (i.e., In, Ga, N, and O) but also for contaminate elements (i.e., C, Na, Al, and Si).

#### 3. Results and discussion

The structural and spectroscopic properties of the InN thin films are presented in Fig. 2. The HRXRD pattern in Fig. 2(a) clearly



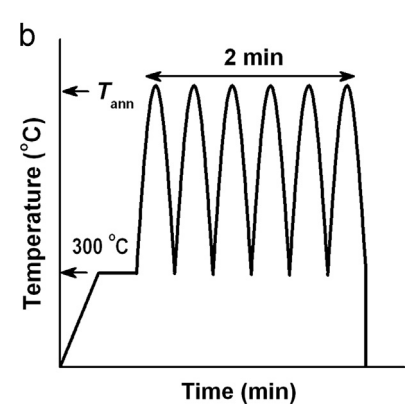


**Fig. 1.** Schematic diagram of thermal annealing temperatures as a function of annealing time employed for the post-growth thermal oxidation of InN thin films; (a) convention rapid thermal annealing (RTA) and (b) cycle-RTA.

reveals the layer structure of InN/InGaN-II/InGaN-II/GaN, where the InGaN-II has a higher In composition due to the increased TMIn flow rate along the growth direction. The reciprocal space mapping (RSM) of the InN/InGaN-II/InGaN-I/GaN structure around the (10–15) atomic planes is shown in Fig. 2(b). It is seen that the InGaN-I layer is coherently strained on the GaN template while the InN layer is completely relaxed. The In composition in InGaN-I is thus obtained in terms of its (0 0 0 2) angle in Fig. 2(a), which is 16%. The feature of InGaN-II is missing in the RSM (10–15) in Fig. 2(b) due to its small thickness, however, it appears in the  $\omega$ -20 HRXRD spectrum measured around InN (10–15) as shown in the inset of Fig. 2(b). This result indicates that the InGaN-II layer is largely relaxed due to its higher In incorporation, which turns out to be 63% by a simple calculation based on the diffraction angle of InGaN-II in Fig. 2(a) assuming it is completely relaxed.

Typical Raman scattering (488-nm excitation) and photoluminescence (PL, 532-nm excitation) spectra measured at room temperature are shown in Fig. 2(c) and its inset, respectively. Both spectra exhibit the typical features of InN [12]; the near-band-edge PL emission at 0.75 eV, as well as the narrow/sharp peaks of PL and Raman features [e.g.,  $E_2^{\rm high} \sim 490~{\rm cm}^{-1}$  and  $A_1({\rm LO}) \sim 592~{\rm cm}^{-1}$ ], indicates that the InN thin film is obtained with high crystal quality. Fig. 2(d) shows a typical scanning electron microscopic (SEM) image of the as-grown InN thin film; an image with a larger magnification is shown in the inset of Fig. 2(d). These SEM images reveal a smooth surface with high density ( $\sim 4 \times 10^9~{\rm cm}^{-2}$ ) nano-sized pits of the resultant InN thin films.

Fig. 3 presents the comparisons between the oxidations of InN at 700 °C employing the RTA (with and without Si<sub>3</sub>N<sub>4</sub> coating) and CRTA methods [see Fig. 1(a) and (b)]. It is seen that bcc-In<sub>2</sub>O<sub>3</sub> crystal with  $In_2O_3$  (2 2 2)//InN (0 0 0 2) formed in both cases but with higher crystal quality in the case of CRTA oxidation in terms of the FWHMs of the In<sub>2</sub>O<sub>3</sub> (2 2 2) peak. Although a Si<sub>3</sub>N<sub>4</sub> surface coating can somehow improve the crystal quality of In<sub>2</sub>O<sub>3</sub>, it gives rise to the emergence of metallic In as indicated by In (101) at about 16.5°. Also seen is that the InN (0002) peak in the RTA oxidations, both with and without the Si<sub>3</sub>N<sub>4</sub> coating, is much weaker than that in the CRTA oxidation. These observations indicate that, from the crystal quality point of view, CRTA is much more advantageous than RTA, which results in higher crystal quality for both the grown In<sub>2</sub>O<sub>3</sub> and the remaining InN. It has to be noted here that there is no intentional oxygen supplied during the post-growth thermal annealing. Thus the oxygen species in the oxidation were due to the environmental contaminations, especially those adsorbed on the surface of InN, where nano-scaled pits are present with high density [see Fig. 2(d)].

A cross-sectional transmission electron microscopy (TEM) image recorded from the CRTA sample is shown in Fig. 4, where it is clearly seen that there are two distinguishable interfaces. One is between  $\rm In_2O_3$  and  $\rm InN/InGaN$  and the other is between  $\rm InN/InGaN$  and GaN. Both interfaces are parallel to the sample surface, implying the layer-by-layer oxidation of InN upon CRTA. The arrow in Fig. 4 indicates the advancing direction of the top interface that initiated at the original surface of InN and moved down towards GaN during the thermal oxidation. This interface, in terms of the HRXRD comparisons in Fig. 3, typically the intensity and line-width of  $\rm In_2O_3$  (2 2 2), is much rougher in the RTA sample than those in the CRTA and  $\rm Si_3N_4$ -capped RTA samples. On the other hand, the metallic In emerged in the  $\rm Si_3N_4$ -capped RTA sample is most likely formed in the area below this interface, i.e., in the InN/InGaN area.

Fig. 5(a) shows the evolution of structural properties of the CRTA oxidation of InN as a function of  $T_{\rm ann}$  ranging from 650 to 750 °C. It is seen that the In<sub>2</sub>O<sub>3</sub> (2 2 2) [InN (0 0 0 2)] peak increases (decreases) monotonically with  $T_{\rm ann}$  while the other peaks do not exhibit apparent changes in intensity. The  $T_{\rm ann}$ -dependant

#### Download English Version:

## https://daneshyari.com/en/article/1329787

Download Persian Version:

https://daneshyari.com/article/1329787

<u>Daneshyari.com</u>